DRAFT VERSION JUNE 25, 2003
Preprint typeset using LaTeX style emulateapj v. 11/12/01

SUPERSOFT X-RAY SOURCES IN M31

R. DI STEFANO[1,2], A. K. H. KONG[1], J. GREINER[3], F. A. PRIMINI[1], M. R. GARCIA[1], P. BARMBY[1], P. MASSEY[4], P. W. HODGE[5], B. F . WILLIAMS[1], S. S. MURRAY[1], S. CURRY[2], T. A. RUSSO[2]

Draft version June 25, 2003

ABSTRACT

We report on luminous supersoft X-ray sources (SSSs) in M31. In a survey which was most sensitive to soft sources in four $8' \times 8'$ regions covered by *Chandra*'s ACIS-S S3 CCD, we find 33 SSSs that appear to belong to M31. Two of these were first identified as SSSs through *ROSAT* observations. Two SSSs may be identified with symbiotics, and 2 with supernova remnants. SSSs in the disk are clustered near star-forming regions, possibly indicating that they are young; SSSs in the outer disk and halo are likely to be old systems. The largest density of bright SSSs is in the bulge; some of the bulge sources are close enough to the nucleus to be remnants of the tidal disruption of a giant by the massive central black hole. By using *Chandra* data in combination with *ROSAT* and *XMM* observations, we find most SSSs to be highly variable, fading from or brightening toward detectability on time scales of months. There is evidence for SSSs with low luminosities ($\sim 10^{36}$ erg s^{-1}). There is also evidence that some SSSs have spectral characteristics mirroring those of the Magellanic Cloud and Milky Way SSSs ($kT \leq 100$ eV); we call these "classical" supersoft sources. Other SSSs may either have small ($< 10\%$) hard components, or slightly higher temperatures (but still < 300 eV). We refer to these SSSs as quasi-soft sources. While white dwarf models may apply to M31 SSSs, some SSSs, including some of the quasi-soft sources, could be accreting intermediate-mass black holes, or neutron stars.

Subject headings: galaxies: individual (M31) — X-rays: binaries — X-rays: galaxy

1. INTRODUCTION

1.1. *Observations of Supersoft Sources*

Very soft X-ray sources, with little or no apparent emission above 1 keV, were discovered in the Magellanic Clouds by the *Einstein* X-Ray Observatory (Long, Helfand, & Grabelsky 1981). The *ROSAT* All-Sky Survey detected approximately one dozen such soft sources in the Magellanic Clouds, while 15 soft sources were discovered during *ROSAT*'s initial survey of M31 (Supper et al. 1997). Later, Kahabka (1999) suggested that 34 M31 X-ray sources could have similarly soft spectra. Astronomers coined the term "luminous supersoft X-ray source" (SSS), and a new class of X-ray sources was born. With no definite physical model, sources were afforded membership based simply on their observable characteristics. In general, there was little or no emission above $1-1.5$ keV; blackbody spectral fits yielded values of kT between 30 and 100 eV; the associated luminosities were $10^{37}-10^{39}$ erg s^{-1}.

Because the soft X-radiation they emit is readily absorbed by the ISM, the *ROSAT* census of SSSs is highly incomplete. Based on the data and models of the gas distribution in M31 and in the Milky Way, Di Stefano & Rappaport (1994) concluded that each of these 2 galaxies likely houses a population of ~ 1000 SSSs with $L \geq 10^{37}$ erg s^{-1} and $kT \geq 30$ eV. Lower luminosity, lower temperature sources, which are less likely to be detected, had not been discovered and were not included in their simulations. Since then however, it has been established that some CVs may turn on as SSSs (Greiner & Di Stefano1999; Greiner et al. 1999; Patterson et al. 1998), exhibiting temperatures (< 30eV) and luminosities ($10^{35}-10^{36}$ergs^{-1}) lower than those of the original set of Milky Way and Magellanic Cloud SSSs. Bright CVs provide a much larger pool (perhaps $\sim 10^4$ in a galaxy like M31) of potential SSSs.

1.2. *Models*

Two circumstances pointed to white dwarf models as promising explanations for SSSs. First, the effective radii for the SSSs discovered in the Galaxy and Magellanic Clouds are comparable to those of white dwarfs (WDs). Second, some hot WDs and pre-WDs have been observed as SSSs (see Greiner 2000), including several recent novae, symbiotic systems, and a planetary nebula (PN). More than half of all SSSs with optical IDs do not however, seem to be examples of systems of known types. It is the mysterious nature of these other systems that has excited much of the interest in SSSs. A promising model is one in which matter from a Roche-lobe-filling companion accretes onto the WD at rates so high ($\sim 10^{-7} M_\odot$ yr^{-1}) that it can undergo quasi-steady nuclear burning (van den Heuvel et al. 1992; Rappaport, Di Stefano & Smith 1994; Hachisu, Kato, & Nomoto 1996, Di Stefano & Nelson 1996). Because matter that is burned can be retained by the WD, some SSS binaries may be progenitors of Type Ia supernovae.

There is indirect evidence in favor of nuclear-burning WD models for several SSSs. The X-ray spectra, e.g., are reasonably well-fit by WD atmosphere models (van Teeseling et al. 1996). There is rough agreement between optical and UV data and predictions based on a reprocessing-dominated disk (Popham & Di Stefano 1996). Finally, the predicted velocities of bipolar outflows (jets) are near the escape velocity of a WD (Southwell et al. 1996, Parmar et al. 1997). Presently, however, there is little direct evidence that the models are correct.

Because the phenomenological definition of SSSs is so

[1] Harvard-Smithsonian Center for Astrophysics, 60 Garden Street, Cambridge, MA 02138; rdistefano@cfa.harvard.edu
[2] Department of Physics and Astronomy, Tufts University, Medford, MA 02155
[3] Max-Planck-Institut für extraterrestrische Physik, Giessenbachstrasse Postfach 1312, D-85748 Garching, Germany
[4] Lowell Observatory, 1400 West Mars Hill Road, Flagstaff, AZ 86001
[5] Astronomy Department, University of Washington, Box 351580, Seattle, WA 98195-1580

broad, it is in fact likely that the class includes objects of several types. Indeed, any object more compact than a WD could certainly act as an SSS. Neutron star models have been considered (Greiner et al. 1991, Kylafis & Xilouris 1993). Although neutron star luminosities and photospheric radii can be large enough to support SSS behavior, there is no well-understood reason why such a large photosphere would be preferred. Intermediate-mass black holes (BHs) are, on the other hand, expected to emit as SSSs, at least if the accretor mass and luminosity is in the appropriate range. (See §8).

We also note that the stripped cores of giant stars that have been tidally disrupted by massive black holes are expected to appear as SSSs for times ranging from 10^3 to 10^6 years (Di Stefano et al. 2001). Several such stripped cores could be present within ~ 1 kpc of the nuclei of galaxies harboring high-mass black holes.

1.3. *SSSs in External Galaxies*

To avoid the worst effects of Galactic absorption, our best hope to study galactic populations of SSSs is to search for them in other galaxies. The advent of *Chandra*, with its good low-energy sensitivity, its superb angular resolution, and its low background, will significantly increase the numbers of known sources and extend our knowledge of the class.

Among external galaxies, M31 can play a unique role, simply because of its proximity. First, the population of low-L sources can best be studied in M31. Second, M31 is the only galaxy in which we can hope to identify optical counterparts to a large fraction of SSSs. This step will allow us to get a better understanding of the natures of SSSs, which is our primary goal. In this paper we report on the SSSs detected by *Chandra* in M31.

1.4. *This paper*

The process we used to select SSSs is described in §3. In §4 we present the spectra of the SSSs from which we have collected the most counts. §5 is devoted to optical IDs, while the variability of the SSSs is examined in §6. The locations of the sources relative to large-scale galaxy features and relative to other stellar populations is discussed in §7. In §8 we discuss sources with somewhat harder spectra, which we call "quasi-SSSs" and in §9 we discuss the low-luminosity sources. §10 is a summary of our conclusions.

2. OBSERVATIONS AND ANALYSES

The data were taken as part of two separate observing campaigns. One was a survey studying 3 distinct regions of the disk. The regions encompass the coordinates of 9 *ROSAT*-detected SSSs; we were able to place the S3 CCD, which is especially sensitive to soft X-radiation, over regions including 5 of these SSSs. These 3 disk fields, which span a wide range of stellar populations, were each observed 3 times (15 ks for each ACIS-S observation) by *Chandra* during 2000–2001, at intervals of 3–4 months.

The second campaign led to superb coverage of the central regions. The central region of M31 was observed by *Chandra* ACIS-I eight times from 1999 to 2001, with exposure times ranging from 4 to 8.8 ks. The details of the observations are given in Kong et al. (2002). The same region was also observed by *Chandra* ACIS-S for 37.7 ks (after rejecting high background period) on 2001 October 5. We make use of this deep *Chandra* observation to search for SSSs near the nucleus. Since the soft X-ray sensitivity is best in S3, we here limit our discussion on the nuclear region to sources detected within this $8' \times 8'$ region.

For each observation, we examined the background and rejected all high-background intervals. Only events with photon energies in the range of 0.1–7 keV were included in our analysis. For the three disk fields, the three observations in each field were merged to increase the signal-to-noise ratio. To detect sources we used CIAO task *WAVDETECT* (Freeman et al. 2002). Source count rates were determined via aperture photometry and were corrected for effective exposure and vignetting. The radius of the aperture was varied with the average off-axis angle to match the 90% encircled energy function. Background was extracted from an annulus centered on each source. In some cases, we modified the extraction region to avoid nearby sources. It was also necessary to modify the extraction radius for some faint sources close to more luminous sources. Every extraction region was examined carefully in the image. All detected sources have signal-to-noise ratio (S/N) > 3, with a minimum of 9 counts. For more details, see Kong et al. 2002. The X-ray sources found in M31's globular clusters (GCs) are discussed in Di Stefano et al. 2002a. A comparative study of the luminosity functions of each region has been carried out (Kong et al. 2003). A preliminary report on the SSSs in M31 can be found in Di Stefano et al. 2002b.

3. SELECTION OF SOFT SOURCES

3.1. *Background*

We used PIMMS to predict that each of the five disk SSSs covered by S3 would be detected in a 15 ksec *Chandra* ACIS-S observation. Our confidence in these predictions was bolstered by the fact that we had completed an AO1 *Chandra* program (PI: Murray) that observed most of the local (Galactic and Magellanic Cloud) SSSs, and that those data had been in almost perfect agreement with the PIMMS predictions.[6] None of the *ROSAT* sources were detected during the first set of *Chandra* observations; no new SSSs with count rates comparable to those expected for the *ROSAT*-discovered sources were discovered. While there were many very soft sources, many of these were foreground stars. Furthermore, most of the soft sources produced a small number of counts and, typically, one or more photons had energy greater than 1.1 keV. Especially because the *ROSAT* PSPC had a lower-energy cut-off than *Chandra*, making spectral comparisons difficult, it was not clear which of the *Chandra*-discovered sources should be designated as SSSs.

We therefore developed an algorithm to select SSSs from among the characteristically low-count-rate sources in external galaxies (Di Stefano & Kong 2003a, b). At this point the algorithm, motivated by our M31 data, has been applied to simulated data and to *Chandra* data from M101, M83, NGC 6947, M51 (Di Stefano & Kong 2003a, b), NGC 4472, M87 (Friedman et al. 2002), and M104 (Di Stefano et al. 2003), and to *XMM* data from NGC 300 (Kong & Di Stefano 2003) and from the halo of M31 (Di Stefano & Kong 2003,c). It successfully selected very soft sources, about a dozen of which have high

[6] The count rates are almost exactly as predicted. An analysis of these data has not yet, however, been published. This is because the *ACIS-S* low-energy calibration is not yet well-enough understood. At the lowest energies, anomalies appear in the spectra of all nearby SSSs. We do not collect enough counts from most extragalactic SSSs for the artifacts to be apparent, but if the calibration is completed, low-count spectra, like the ones we present in §4, should be checked.

enough luminosities that their spectra can be computed to confirm that the spectral models are dominated by a highly luminous soft component. The algorithm is described in detail in Di Stefano & Kong 2003a, b. Below we provide a brief sketch.

3.2. *Algorithm to select soft sources*

The first step is to impose a set of strict hardness ratio conditions. We use 3 energy bins to define hardness ratios: **S:** 0.1-1.1 keV, **M:** 1.1-2 keV, **H:** 2-7 keV. We consider 2 hardness ratios, HR1 and HR2, demanding that

$$HR1 = \frac{M-S}{M+S} < -0.8 \quad (1)$$

and

$$HR2 = \frac{H-S}{H+S} < -0.8. \quad (2)$$

These conditions imply that $S > 9M$, and $S > 9H$. The so-called "HR" conditions consist of the above conditions, plus 2 additional criteria: $(S+\Delta S) > 9(M+\Delta M)$, and $(S+\Delta S) > 9(H+\Delta H)$, where ΔS, ΔM, and ΔH are the one-σ uncertainties in S, M, and H, respectively. Sources satisfying these 4 conditions are denoted "SSS-HRs". The designation SSS-HR requires that the S band receive more than 13.1 photons if no photons arrive in either the M or H bands, while S must receive more than 24 photons if there is even a single photon in either M or H. (See Di Stefano & Kong 2003a, b for details and applications to both simulated and real data.)

Sources with identical spectral characteristics to those satisfying the HR conditions may not be able to satisfy these conditions if their count rates are low, especially if one or more photons falls in the M or H bands. We can successfully identify some such sources by relaxing the conditions. If a source satisfies conditions (1) and (2), it is an SSS which we designate "3σ".

It makes sense to relax the conditions further. Consider for example, a source with 100 eV, which could correspond to a nuclear-burning WD with mass close to the Chandrasekhar limit. Such a source does emit some photons above 1.1 keV. If it lies behind a large gas column, emission in the S band can be significantly eroded, allowing the hardness ratio, HR1, to have a large value. That is, even if we are primarily interested in sources that have spectra like those of the first batch of SSSs discovered in the Galaxy and Magellanic Clouds, we need to loosen the selection criteria and risk also selecting sources that are somewhat harder. The selection of harder sources could be advantageous, even for the selection of nuclear-burning WDs, since so far we have only 9 candidates for the model. It is unlikely that the spectral properties of these 9 sources span the full gamut of model properties. It is feasible, e.g., that in some WD systems, hot coronae or interactions with a dense interstellar medium could produce a small hard component. In addition, if some SSSs are neutron star or black hole systems, they may occasionally emit harder radiation or even exhibit a power law tail that carries a small fraction of the energy.

We will therefore call a source a classical supersoft source if it provides enough counts to allow a spectral fit and if any of the following conditions are met. (1) The spectrum is well-fit by a blackbody model with $kT < 175$ eV, (2) The spectrum is well-fit by a power-law model with $\alpha \geq 3.5$, (3) Whatever the best fit model, less than 10% of the energy is carried by photons with energy greater than 1.5 keV. (See Di Stefano & Kong 2002a.)

Since we cannot fit spectra for most X-ray sources in external galaxies, we designed the algorithm mentioned above (Di Stefano & Kong 2003a, 2003b). Our algorithm consists of a sequence of selection procedures, starting with those that select SSS-HR and SSS-3σ sources. SSSs selected by each procedure are given a label corresponding to the procedure. When tested on simulated and real data (Di Stefano & Kong 2003a, 2003b), each procedure selected sources with spectra similar to those of the SSSs that have been discovered in the Magellanic Clouds and in the Milky Way (i.e., the classical SSSs). In addition, however, each procedure (including HR and 3σ) also selected some harder sources. Some sources might, e.g., have a power law tail, others might be blackbodies with kT = 250 eV. If, therefore, we could collect enough photons from each extragalactic X-ray source to fit a spectrum, some of our sources in each category would satisfy the definition for classical SSSs, and others would be somewhat harder. We refer to these harder sources as quasi-soft sources. We cannot say *a priori*, which of the sources selected by which procedure are classical SSSs and which are quasi-soft. (But see §8.) We note that a larger fraction of sources selected by the less restrictive criteria are likely to be quasi-soft, while almost all sources selected by HR and 3σ are likely to be classical supersoft sources.

In Table 1 we list all of the sources selected by our algorithm. The procedure that selected this source is listed in column 10. This will allow future studies to focus on any set of sources deemed appropriate. See Di Stefano & Kong (2003a, b) for a definition of each category. Note, however, that the selection criteria alone cannot be used to distinguish between classical supersoft sources and quasi-soft sources. The designation "SSS" must therefore include both.

Note that, although the selection of quasi-soft sources was not one of our original goals, these sources are likely to be very interesting in their own right, as most do not seem to correspond to known classes of X-ray sources. Note also that the distinction between classical SSSs (cSSs) and quasi-soft sources (qSSs) is phenomenological and not physical. Some nuclear-burning WDs, e.g., may be qSSs, some accreting intermediate-mass BHs may be cSSs. The notion of qSSs is introduced to recognize that the SSSs selected by our algorithm encompass a wider group of sources than the "classical" SSSs found locally. All SSSs selected by our algorithm are listed in Table 1.

4. SPECTRA

We examine the energy spectra of bright SSSs. Only those in the central region provide enough counts for a reasonable spectral fit. Figure 2 shows four representative spectra. It is worth noting that the degradation of soft energy (< 1 keV) sensitivity might affect the spectral fits significantly and we therefore correct the response matrices to take this effect into account. r2-12 is the brightest SSS in M31 and is seen in every *Chandra* observation; it was also detected by previous *ROSAT* observations (Supper et al. 1997, 2001; Primini et al. 1997). A single blackbody model cannot provide a good fit; there is an excess above ~ 1 keV. From archival *XMM-Newton* observations, r2-12 shows a high energy tail up to ~ 5 keV (Kong et al., in preparation). We therefore add an additional powerlaw component (fixed at α = 2) to improve the fit. For r1-9, the spectrum also requires a two-component model (blackbody + powerlaw) to achieve a good fit. r1-25 is fit by a blackbody model with kT = 122 eV, while r1-n1 is well fit by a model with kT = 25 eV.

TABLE 1

SSS SOURCE LIST

Object	R.A. (h:m:s)	Dec. (°:′:″)	Soft Counts	Medium Counts	Hard Counts	HR1[a]	HR2[b]	Count Rate (10^{-3})	Category	d (″)
f1-26	00:38:40.6	+40:19:57.7	45.04	0.00	1.23	-1.0	-0.95	1.17	HR	59
f1-27	00:38:23.9	+40:25:27.9	28.51	23.37	2.72	-0.1	-0.83	1.38	HR1	113
f1-28	00:38:18.9	+40:15:33.5	2.28	11.05	0.68	0.66	-0.54	0.35	med	53
f1-62	00:38:38.7	+40:15:11.3	9.70	1.03	0.00	-0.81	-1.0	0.27	noh	74
f1-10	00:38:25.7	+40:17:39.4	8.70	0.92	1.52	-0.81	-0.70	0.28	3σ1	33
f1-7	00:38:31.2	+40:17:12.0	31.52	3.09	0.00	-0.82	-1.0	0.87	3σ	60
f1-29	00:38:14.0	+40:15:22.9	36.06	4.32	0.00	-0.79	-1.0	1.02	3σ	57
f1-46	00:38:02.9	+40:08:26.3	43.17	6.17	6.30	-0.75	-0.75	1.40	3σ	83
f1-37	00:39:38.7	+40:11:00.4	190.41	36.79	0.00	-0.68	-1.0	5.74	mnoh	120
f2-24	00:41:49.2	+40:56:43.8	68.00	0.75	1.49	-0.98	-0.96	1.83	HR	55
f2-33	00:41:39.9	+41:04:25.7	18.23	7.92	0.00	-0.39	-1.00	0.68	snoh	27
f2-52	00:41:36.5	+41:00:17.6	8.44	3.88	0.74	-0.37	-0.84	0.34	noh	50
f2-53	00:41:35.6	+41:06:56.8	57.75	8.10	5.45	-0.75	-0.83	1.86	3σ	70
f2-91	00:41:41.9	+41:07:16.7	32.63	0.00	4.96	-1.00	-0.74	0.98	3σ	70
f2-26	00:41:43.5	+41:05:05.4	228.38	37.94	2.39	-0.72	-0.98	7.03	HR1	56
f2-56	00:41:18.5	+40:52:00.0	393.10	189.17	25.36	-0.35	-0.88	15.91	σ	120
f2-72	00:42:12.8	+41:05:58.9	45.60	0.00	0.00	-1.00	-1.00	1.19	HR	50
f3-8	00:46:16.7	+41:36:56.0	61.95	14.79	3.65	-0.61	-0.89	2.10	σ	92
f3-29	00:46:14.6	+41:43:18.3	5.49	2.75	0.49	-0.33	-0.84	0.22	noh	25
f3-31	00:45:58.1	+41:35:02.2	23.57	21.68	0.00	-0.04	-1.00	1.18	med	68
f3-46	00:46:23.7	+41:37:51.6	10.85	2.86	1.11	-0.58	-0.81	0.38	noh	82
f3-48	00:46:04.1	+41:49:42.7	25.39	2.36	0.96	-0.83	-0.93	0.75	3σ	108
f3-66	00:47:33.3	+41:35:11.6	138.57	26.15	0.00	-0.68	-1.00	4.31	med	154
f3-2	00:46:29.1	+41:43:13.9	33.65	4.16	3.63	-0.78	-0.81	1.08	3σ	61
f3-13	00:46:05.7	+41:43:04.7	28.63	6.28	0.75	-0.64	-0.95	0.93	snoh	28
f3-15	00:46:04.6	+41:41:23.7	20.24	8.34	0.48	-0.42	-0.95	0.76	snoh	63
f3-26	00:46:39.0	+41:39:07.5	19.23	7.66	1.64	-0.43	-0.84	0.74	HR1	115
r1-25	00:42:47.8	+41:15:49.6	188.58	15.82	0.00	-0.85	-1.00	5.43	HR	16
r1-9	00:42:44.3	+41:16:07.3	675.26	235.72	47.00	-0.48	-0.87	25.47	σ	~ 1
r2-12	00:42:52.4	+41:15:39.7	2593.80	11.52	0.14	-0.99	-1.00	69.29	HR	26
r2-19	00:42:43.2	+41:13:19.2	384.01	89.68	9.29	-0.62	-0.95	12.84	σ	30
r2-42	00:42:36.5	+41:13:50.0	33.75	7.79	0.00	-0.62	-1.00	1.10	snoh	45
r2-54	00:42:38.6	+41:15:26.3	17.55	0.51	0.09	-0.94	-0.99	0.48	3σ	24
r2-56	00:42:50.4	+41:15:56.2	40.41	0.71	0.80	-0.97	-0.96	1.11	HR	26
r3-11	00:43:14.3	+41:16:50.1	18.31	15.48	0.74	-0.08	-0.92	0.91	med	23
r1-n2	00:42:43.0	+41:16:03.9	130.94	4.58	0.00	-0.93	-1.00	3.60	HR	8
r2-n1	00:42:43.9	+41:17:55.5	135.71	0.00	0.00	-1.00	-1.00	3.60	HR	19
r2-n2	00:42:47.3	+41:15:07.2	95.29	0.77	1.39	-0.98	-0.97	2.59	HR	18
r2-n3	00:42:39.2	+41:14:24.4	8.91	9.88	0.66	0.05	-0.86	0.51	med	5
r2-n4	00:42:59.3	+41:16:42.8	115.79	0.00	0.00	-1.00	-1.00	3.07	HR	37
r2-n6	00:42:47.0	+41:14:12.4	20.44	0.96	0.00	-0.91	-1.00	0.56	3σ	23
r3-n1	00:42:49.0	+41:19:47.1	6.64	2.56	0.62	-0.44	-0.83	0.26	med	64
r3-n2	00:43:06.9	+41:18:09.0	50.49	0.00	0.00	-1.00	-1.00	1.34	HR	37

[a] $HR1 = (M-S)/(M+S)$
[b] $HR2 = (H-S)/(H+S)$

Column 1: source name. **Columns 2 & 3:** right ascension and declination. **Columns 4, 5, & 6:** the number of soft, medium and hard X-ray counts detected for each source. Source count rates were determined via aperture photometry and were corrected for effective exposure and vignetting. **Columns 7 & 8:** hardness ratios, see §3.2. **Column 9:** counts per second. **Column 10:** selection criterion by which the source was selected as an SSS. (See Di Stefano & Kong 2003a, b.) **Column 11:** angular distance to the nearest X-ray source.

5. SOURCE IDS

We attempted to identify the SSSs with sources observed at other wavelengths to (1) search for possible counterparts, and (2) distinguish between M31 SSSs and sources that may be associated with foreground or background objects.

Chandra's good angular resolution, in combination with the spectral sensitivity of ACIS-S can be crucial for this task. Time variability can also be helpful. Consider two SSS counterparts suggested by previous or ongoing work. One is a nova, associated with a *ROSAT* SSS (Nedialkov et al. 2002). Because the spatial resolution of *ROSAT* makes the correspondence difficult to establish, the timing of the nova and the apparently coordinated optical and X-ray decline play a crucial role in supporting the identification. More recently (Williams et al. 2003), an association has been suggested between a *ROSAT*-observed recurrent transient, (White et al. 1995) an X-ray source observed by *Chandra-HRC*, and an SNR. The time variability of the X-ray source would seem to be incompatible with the SNR interpretation. Clearly a verification that the *HRC*-observed source is an SSS would be important.

5.1. *Search for Matches*

We have searched for correlations between the SSSs and all cataloged objects, we have examined images from *The Local Group Survey* (LGS) the *Digital Sky Survey* (DSS), and from *HST*. There are a number of *HST* images containing SSS positions near the center of M31, but few images of the disk. Fortunately, the LGS and the DSS complement the *HST* observations, with the combination of these 2 optical surveys providing good coverage of most of the disk.

5.1.1. *HST*

We searched the HST archive for WFPC2 images whose centers were within $4'$ of the position of each SSS listed in the caption of Table 3. Because of the irregular WFPC2 footprint, not all such images would necessarily cover the coordinates of the object, so we retrieved the images from the archive, created cosmic-ray rejected 'stacked' images, and checked the object positions in each image. We found that images taken with the UV F160BW filter were essentially blank everywhere, with no indication of stars or even the galaxy nucleus, so we did not consider them further. The HST datasets in which the supersoft sources appear are shown in Table 3.

To identify possible optical counterparts to the supersoft sources, we used DS9 to mark the object positions on the images, and then visually inspected them. Since all of the positions were close to the center of M31, the error circles contain many faint stars, any (or none) of which could be the true optical counterpart of the supersoft source. Almost none of the error circles contained optical sources which were significantly brighter than the typical stellar background. To quantify the detection limits, we measured the background σ at the location of each object in each WFPC2 image and computed the magnitude (in the WFPC2 bandpass "Vegamag" system) corresponding to an object with a 20σ flux. The resulting limits appear in Table 3.

Two supersoft sources were detected in HST images. r1-n2 appears as an optical transient in the HST datasets u2lg020 and u2lh010; these data were obtained in June 1995. No optical transient appears in other images which cover the same position, including u2c7010 (September 1994), u2e2010 (October 1994), and u5lt010 (February 2000). The optical magnitudes of the transient are given in Table 1. (See also Kaaret 2002.)

r2-56 was identified with planetary nebula 462 in the catalog of Ciardullo et al. (1998), but, since it is resolved at X-ray and radio wavelengths, it is more likely to be a supernova remnant (SNR; Kong et al. 2003) Although its coordinates are located within many of the HST images, it is only visually apparent in a narrow-band Hα image (see Figure 3). The Hα magnitude is given in Table 3.

5.1.2. *Optical Surveys*

We examined *The Local Group Survey* (LGS) and Digital Sky Survey (DSS) images containing the coordinates of each SSS. *The Local Group Survey* project uses the 4-m telescopes of NOAO for an optical survey of all the Local Group galaxies currently forming stars, in *UBVRI* and the narrow-band nebular filters Halpha, [OIII], and [SII]. These data have spatial resoluton of 1 arcsec and go to a S/N of 10 at $U = 24.5$, $B = V = R = I = 25.0$, with good astrometric ($0.3''$) accuracy.

For the DSS images, we examined the images for each source visually and then extracted the magnitude from the USNO catalog (Monet 1998).

5.1.3. *M31 Catalog*

Table 2 summarizes the results of matching our new *Chandra* source catalog with existing catalogs of M31 X-ray sources (Supper et al. 1997, 2001). Due to the poorer spatial resolution of the *ROSAT* PSPC, we used a relatively large searching radius ($15''$) to cross-correlate with the *Chandra* catalog.

5.2. *Matches*

5.2.1. *Supernova Remnants*

Supernova remnants (SNRs) can have very soft X-ray spectra. To identify those SSSs which are SNRs, we first checked for matches between the SSSs and SNRs that have been previously identified through optical and radio surveys. We found 2 matches.

Optical and radio and X-ray observations (Kong et al. 2003) have resolved r2-56, solidly establishing that it is an SNR. Yet, this source is one of the softest XRSs in our sample, with no emission above 1.1 keV. This clearly indicates that we cannot eliminate SNRs from any sample of spectrally selected soft sources simply by tightening the eligibility criteria to include only the softest sources. The Field 2 source f2-53 is also identified as an SNR through optical observations (Magnier et al. 1997).

Are these 2 SNRs the only ones among our list? Certainly they are the only ones identified through matches at other wavelengths. But, because the relative signature in X-ray, optical, and radio can vary, depending on the environment of the supernova progenitor, it is possible that some X-ray active SNRs could be missed at other wavelengths. It is therefore important to have a second discriminant. Fortunately, time variability provides a second test. Because the X-ray emission from an SNR presumably emanates from an extended region, it should not vary significantly (e.g., by a factor of 2) over periods much smaller than years. Neither r2-56 nor f2-53 satisfied our criteria for variability.

5.2.2. *Symbiotics*

In symbiotics, wind from a giant star carries mass to a WD companion at rates high enough that nuclear burning can occur.

TABLE 2
SSS VARIABILITY AND OPTICAL IDS

Source	Optical ID	Upper Limit	S-Value	*Chandra*	*XMM*	Note
f1-26		21.6	3.17	v	···	*ROSAT*
f1-27		21.8	···		···	
f1-28		21.6	1.09		···	
f1-62		···	2.53	t	···	
f1-10	$B = 21.1; V = 19.4$		1.98		···	possible symbiotic
f1-7	$B = 16.3; V = 15.6$		1.69		···	
f1-29	$V < 15$		0.12		···	saturated star
f1-46	$V < 15$		3.13	v	···	saturated star
f1-37	$V < 15$		···		···	saturated star
f2-24		···	7.72	v,t	off	
f2-33		···	3.24	v,t	off	
f2-52		···	0.75		on	
f2-53			2.71		on	SNR
f2-91		···	2.01	t	off	
f2-26	$B = 12.2; R = 11.2$		2.36		on	USNO star
f2-56	$B = 13.4; R = 12.2$		0.51		on	USNO star
f2-72	$B = 18.7; R = 18.4$		···		off	USNO star
f3-8		···	1.23		···	
f3-29		···	0.27		···	
f3-31		21.8	0.32		···	
f3-46		21.8	1.18		···	
f3-48		21.8	1.06		on	
f3-66		···	···		···	
f3-2	$B = 19.9; V = 18.4$		1.57		···	
f3-13	$B = 20.2; V = 18.7$		1.62		···	
f3-15	$B = 19.1; V = 17.6$		1.13		···	
f3-26	$B = 19.0; V = 17.6$		3.01	v,t	···	
r1-25		*HST*	2.83		off	
r1-9		···	7.16	v,t	···	unresolved with *ROSAT* and *XMM*
r2-12		*HST*	5.92	v	on[b]	*ROSAT*
r2-19	$I = 18.3$[1]		2.56		on[b]	
r2-42		···	2.32		on[b]	
r2-54		*HST*	1.53		off	
r2-56			1.71		off[c]	SNR[2]
r3-11		20.1	2.16		off	
r1-n2				t	off	S And[3]
r2-n1		19.5,*HST*		t	on[a]	
r2-n2		*HST*		t	off	
r2-n3		···		t	off	
r2-n4		19.5		t	off	
r2-n6		···		t	off	
r3-n1		19.5		t	off	
r3-n2	$B = 23.3; V = 22.0$			t	off	possible symbiotic

Note. — Except f2-26, f2-56, f2-72, and r2-19, photometry of stars is derived from the LGS.
References. —[1] Haiman et al. 1994; [2] Kong et al. 2003; [3] Kaaret 2002
[a] On during the 2nd two (of four) *XMM* observations
[b] On during each of four *XMM* observations
[c] Near the nucleus and an extended X-ray object. It is highly contaminated by the diffuse emission.

Dots indicate that no relevant information was available. **Column 1:** source name. **Column 2:** Optical ID; magnitudes of the USNO stars are taken from the USNO catalog, I magnitude of r2-19 is from Haiman et al. 1994; all others are from the LGS. **Column 3:** Optical V-band upper limits from the LGS; entries marked *HST* should be checked in Table 3. **Column 4:** S is the variability factor defined in the text; $S > 3$ has been taken to denote variability. **Column 5:** Variability as determined within the *Chandra* data set; v denotes variable, t indicates that the source was below the detectability limit at least once. **Column 6:** "on" and "off" indicate whether the source was detected or not by a visual inspection of the *XMM* data. **Column 7:** Notes; *ROSAT*=detected with *ROSAT*, "unresolved" means could not be resolved from the nuclear source.

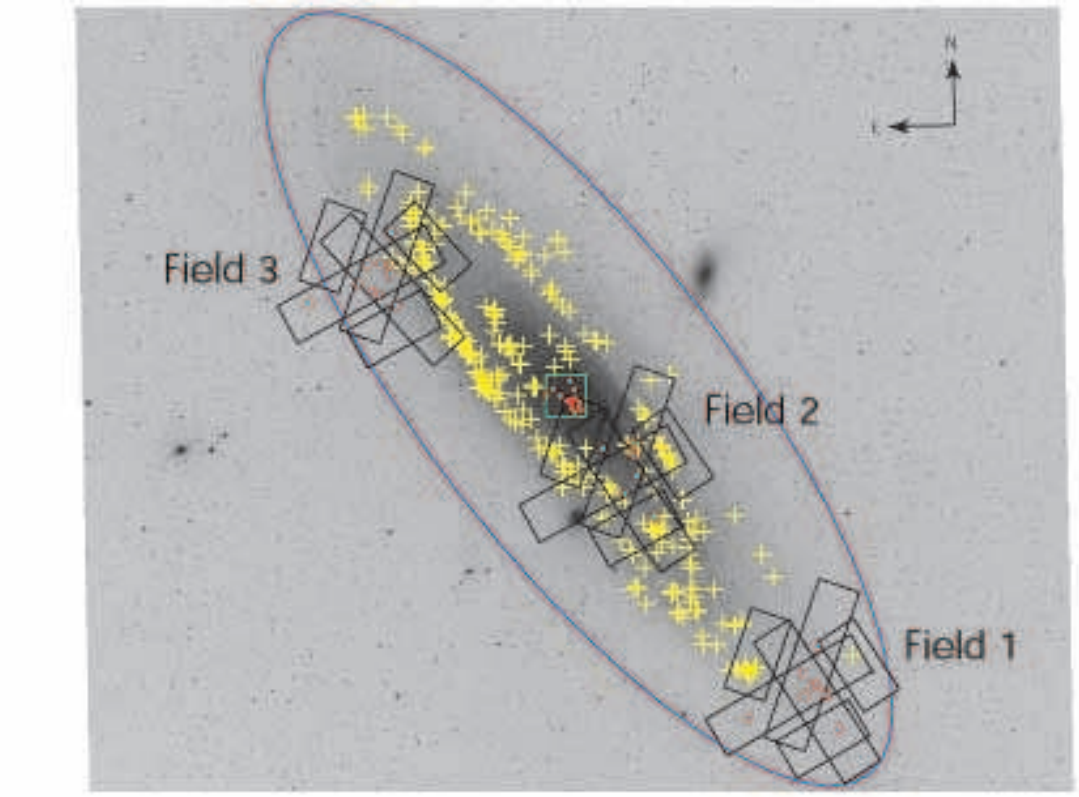

FIG. 1.— Detected SSSs (red dots) overlaid on an optical Digitized Sky Survey image of M31. The fields of view of the three *Chandra* ACIS-S in the disk (black boxes) and the central region (green box) are also shown. Also shown in the figures are the optical position of SNRs (yellow plus signs). The ellipse shows the D_{25} isophote.

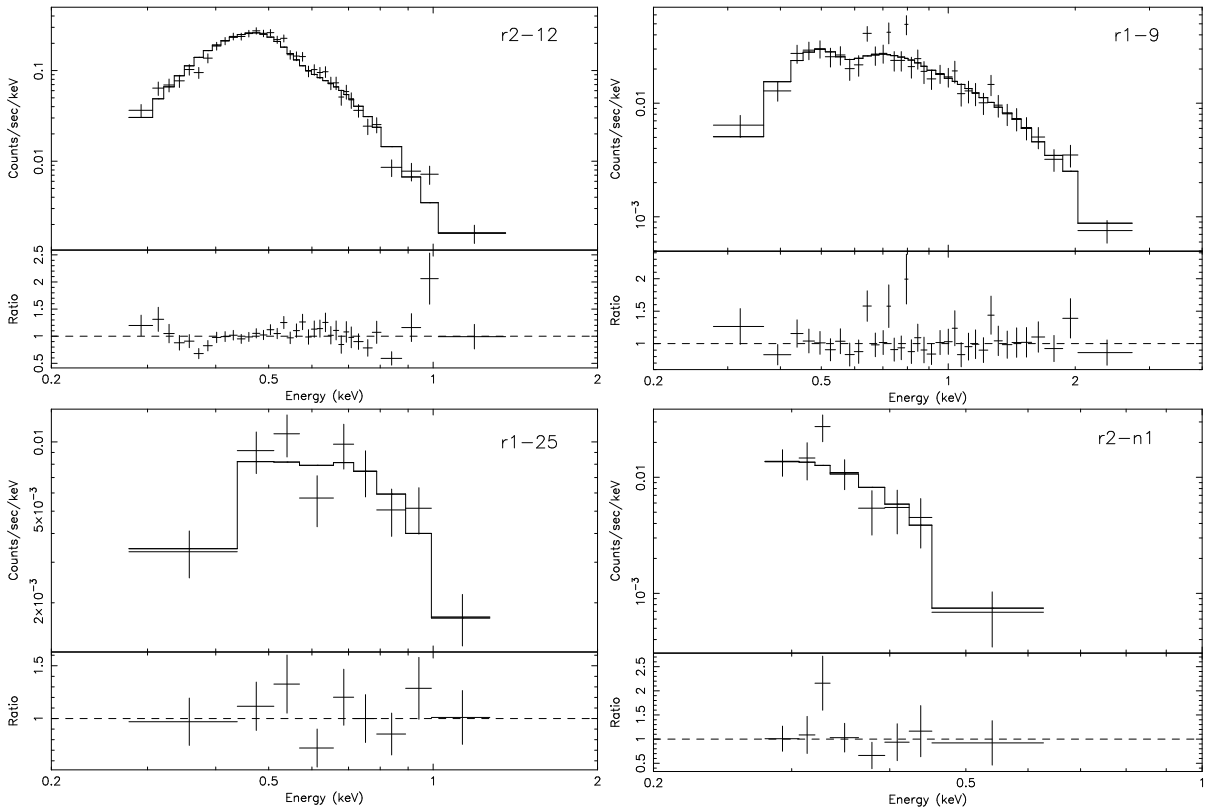

FIG. 2.— Spectral fit to **r2-12** (blackbody + power-law model with $N_H = 2.4 \times 10^{21}$ cm^{-2}, $kT = 56$ eV and $\alpha = 2$ (fixed); $L_{0.3-7} = 4.9 \times 10^{38}$ erg s^{-1}), **r1-9** (blackbody + power-law model with $N_H = 2 \times 10^{21}$ cm^{-2}, $kT = 89$ eV and $\alpha = 3.3$; $L_{0.3-7} = 3.3 \times 10^{37}$ erg s^{-1}), **r1-25** (blackbody model with $N_H = 1.1 \times 10^{21}$ cm^{-2} and $kT = 122$ eV; $L_{0.3-7} = 3.6 \times 10^{36}$ erg s^{-1}), and **r1-n1** (blackbody mode with $N_H = 1.1 \times 10^{21}$ cm^{-2} and $kT = 25$ eV; $L_{0.3-7} = 1.5 \times 10^{37}$ erg s^{-1}.

TABLE 3
HST DATA FOR M31 SSS CANDIDATES

Source	Dataset names	F300W	F336W	F547M	F555W	F656N	F841W	F1042M
r1-25	u2c7010, u2e2010, u2lg020, u2lh020	22.2	20.3	22.5	22.5	21.0	21.0	19.7
r1-n2	u2c7010, u2e2010, u2e2020, u5lt010	···	21.5	23.3	23.4	21.9	21.9	20.0
	u2lg020, u2lh020 (detection)	17.5	17.5	···	18.5	···	18.0	···
r2-12	u2c7010, u2lh010	···	20.3	22.8	···	21.8	···	···
r2-54	u2e2020, u2kj010, u5lt010	···	21.5	···	22.9	···	21.2	···
r2-56	u2c7010, u2e2010, u2lg020, u2lh020	22.2	20.3	22.7	23.1	16.9[a]	21.4	19.9
r2-n2	u2lg020, u2lh010	22.2	20.3	···	22.7	···	21.2	···
r2-n1	u2e2020	···	···	···	23.1	···	21.5	20.0
r3-16	u6d5030 (M. Garcia, proprietary)	···	···	···	···	···	···	···

[a] Object is detected in this filter

We studied each image of each region that had been observed by *HST* and which included locations of the following SSSs; f2-72, f1-25, r1-9, r2-12, r2-19, r2-42, r2-56, r1-n2, r2-n1, r2-n2.

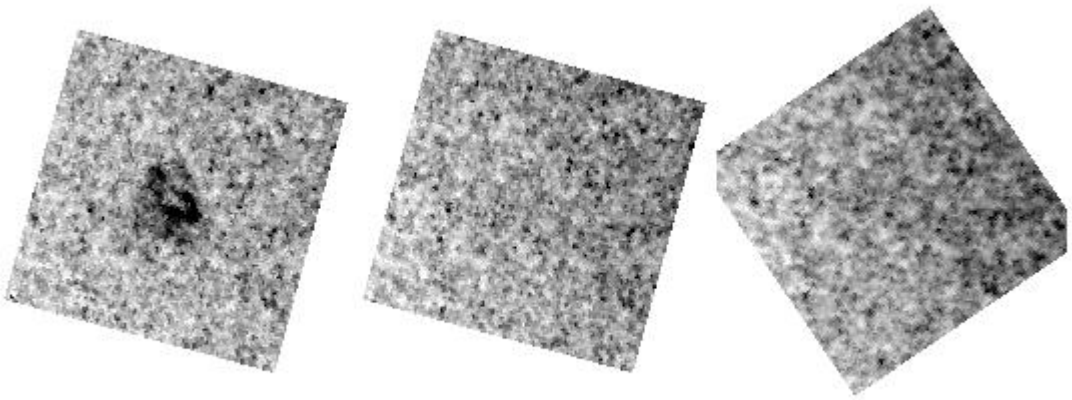

FIG. 3.— *HST* images showing the supernova remnant, r2-56. All images are 10″ on a side and are aligned with north up and east to the left. The left image is in filter F656N (a narrow-band Hα filter), the middle one is in F547M (a medium-band filter similar to Strömgren *y*), and the right-hand image is in the F555W filter (the broadband filter usually used to match the *V* band).

Of the 22 SSSs found in the Galaxy and Magellanic Clouds, 3 are symbiotics. Morgan (1996) gives the range for symbiotics in the LMC as V: 14.7-16.5, with B-V: 0.3-1.7. The V magnitude roughly translates to V: 20.1-21.9 at M31 distances.

Analysis of the LGS data finds a star with $V = 22, B-V = 1.3$ at the location of r3-n2. This system is in a crowded region, and the optical identification is difficult to make by eye; it was identified by an automated process. Using HST images, we find that a star is detected at the 4.6σ level, at RA = 0:43:06.8669, Dec = 41:18:08.758, with $U = 23.57 \pm 0.24$. The field is crowded enough that there is about a 25% chance that this is a chance match. Although there are uncertainties about the identification in each data set, the combination is promising.

In Field 1, which is the least crowded M31 field we have observed, f1-10 is identified with a star in the LGS, having V=19.4, B-V=1.7. Although this system is half a magnitude brighter than the range indicated by Morgan, that range was based on the study of only 10 systems. f1-10 should therefore be considered as a candidate symbiotic.

5.3. *Foreground Stars and Other Contaminants*

Table 2 illustrates that foreground stars are significant contaminants. We have assumed that any bright star found at the position of an SSS is a foreground star. Because f1-10 and r3-n2 have colors and magnitudes that place them in the range of M31 symbiotics, we consider that they may belong to M31. The magnitudes of some other stars in Table 2 may also be consistent with M31 membership. While these may therefore warrant further investigation, for now we consider that they are likely foreground stars

After the elimination of foreground stars, the number of SSSs remaining in our disk fields is small ($5-6$ each in Fields 1, 2, and 3). It is important to estimate the likely contribution of any contaminants, such as foreground intermediate polars, or distant luminous background sources, that may contribute to the non-stellar sources not already identified.

Some background objects, including some distant AGN, may be identified at other wavelengths. In other cases, an identification may be ambiguous. Consider, e.g., f2-52. This is one of the dimmest X-ray sources in our sample (~ 13 counts). It satisfies the "noh" criteria, meaning that it does not have a significant detection, in the H band ($2-7$ keV), although, in this case, there is a $> 1\sigma$ detection in the M band ($1.1-2$ keV). This source is identified with a globular cluster, Bo 251. Although we knew of this identification when we published work on X-ray sources in M31 GCs (Di Stefano et al. 2002), we did not include this association in the GC list, because it is not clear that the optical object is indeed a GC. It may be a more distant galaxy or cluster of galaxies, or it may be something else. This is the only such object we are aware of in the disk fields.

Accreting polars or other soft (but optically dim) XRSs located in the Milky Way's disk or halo can be more difficult to eliminate, especially if the donor is a low-mass star and the disk is small or non-existent.

To estimate the level of contamination from all non-M31 sources which have not been identified at other wavelengths, we have studied data analyzed by the *ChaMP* collaboration. We searched their archives for publicly available analyzed ACIS-S data on fields that (1) have been observed for at least 10 ksec, and (2) that do not contain clusters (GCs or galaxy clusters), gravitational lenses, or nearby galaxies. The energy bins used by *ChaMP* (http://hea-www.harvard.edu/CHAMP/) are slightly different from the ones we have used ($S_{ch} = 0.3-0.9$ keV; $M_{ch} = 0.9-2.5$ keV; $H_{ch} = 2.5-8$ keV). We nevertheless used them exactly in the manner described in §2 to select SSSs. In each of the 4 fields we studied, we found $1-3$ sources per field that satisfy the SSS criteria. These numbers are consistent with the expected numbers of foreground stars. This indicates that SSS interlopers not visible at other wavelengths are rare, a result consistent with previous surveys (see, e.g., Becker 1997, PhD thesis).

6. VARIABILITY

To quantify the level of X-ray variability, we have taken three steps: we searched for the *ROSAT*-observed SSSs in the *Chandra* data set; we searched for the *Chandra*-observed SSSs in the *XMM* data set; we compared the sets of SSSs observed by *Chandra* during different observations of the same field.

6.1. *ROSAT sources in Chandra fields*

M31 was observed by *ROSAT* in 1991 and 1992.[7] *Chandra* observations occurred $9-10$ years afterward, so the combination provides information about variability on the time scale of roughly one decade.

We checked the position of every known SSS observed by *ROSAT*, to determine if it was in a *Chandra*-observed field and, if so, whether it was detected. Eight of the sources should have been detected (yielding 20-150 counts) by *Chandra* during the ~ 15 ksec observations that we conducted. [8]

Field 1: Three *ROSAT* sources are in Field 1. The position of one of the sources (RX J0037.4) was checked only once, and the source was not detected. Two additional sources were located in S3; each was observed 3 times. One of these 2 sources (RX J0038.5) was never detected by *Chandra*; the second (RX J0038.6) was detected in March 2001, but not during the other 2 observations.

Field 2: *ROSAT* identified 1 source in Field 2; RX J0041.8 was located in S3, and was not detected in any of the 3 *Chandra* observations.

Field 3: Five *ROSAT* sources are in Field 3. Of these 5, RX J0047.6, would not have been detectable in a 15 ksec *Chandra* observation, unless the count rate was higher than it had been during the *ROSAT* detection. We might have expected two other sources to be detected as very weak sources, (a few counts per *Chandra* observation), because the *ROSAT* count rates were small, and the sources (RX J0045.4 and RX J0046.1) were not in S3. Two other sources (RX J0046.2+4144 and RX J0046.2+4138) would have been clearly detected if their flux had been comparable to that measured by *ROSAT*. None of the *ROSAT* sources were detected by *Chandra*.

Nuclear region: *ROSAT* detected one SSS in the nuclear region, but the uncertainty in its position is too large to resolve it from 2 SSSs detected by *Chandra.*

6.2. *Chandra sources in XMM fields*

M31 has been observed by *XMM* several times since 2000. In particular, the central $\sim 15'$ region was observed 4 times (2000

[7] All of the published sources were observed in 1991; any variations between 1991 and 1992 have not been discussed in the literature.

[8] The single *ROSAT* SSS that would not have been detected is RX J0045.4; the *ROSAT* count rate was $< 10^{-5}$, and the source was far off-axis in the *Chandra* observation.

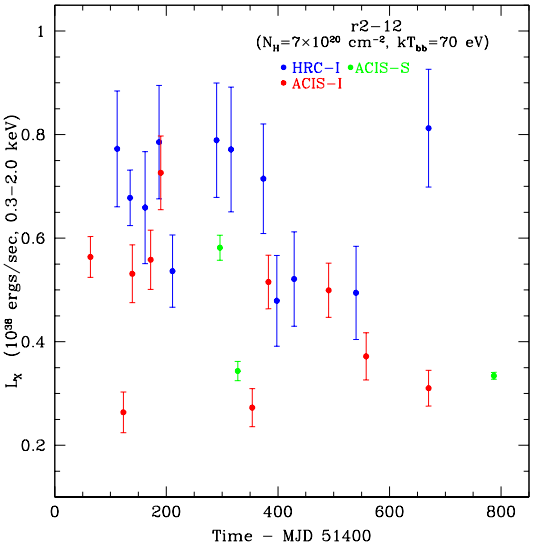

FIG. 4.— Long-term light curve of the brightest SSS, r2-12, spanning from 1999 November to 2001 October. A blackbody spectral model (kT = 70 eV and $N_H = 7 \times 10^{20}$ cm^{-2}) is assumed to derive the 0.5–7 keV luminosity.

June for 30 ks, 2000 December for 12 ks, 2001 June for 39 ks, and 2002 January for 64 ks). Four regions located along the major axis of the disk were each observed once in 2002 January for 60 ks (for instance, see Trudolyubov et al. 2002). For each field, we removed high background periods and combined all three *XMM* detectors (MOS1 + MOS2 + pn) into a composite image. We then visually inspected the composite *XMM* images in each region containing a *Chandra* SSS. The results are summarized in Table 2. Fifteen sources that had been detected by *Chandra* were not detected by *XMM*.

6.3. *Variability Detected by it Chandra*

For all sources observed more than once by *Chandra* we computed a variability parameter following Primini et al. (1993):

$$S(F_{\rm max} - F_{\rm min}) = \frac{\left| F_{max} - F_{min} \right|}{\sqrt{\sigma^2_{F_{max}} + \sigma^2_{F_{min}}}} \qquad (3)$$

where F_{min} and F_{max} are the minimum and maximum X-ray fluxes observed and σ_{min} and σ_{max} are the corresponding errors. Sources with $S > 3$ are marked as variables, v, in Table 2. Note that if a source provides fewer than ~ 10 counts it cannot satisfy the variability criterion, even if it is not detected in the other observations. Some sources were detected in one or more *Chandra* observations, but provided no counts above what was expected from background in at least one observation. These sources are marked with a "t" in Table 2.

6.4. *Summary*

All 8 of the *ROSAT*-discovered SSSs in our disk fields that could have been detected by *Chandra* are transients.

Thirteen of 16 SSSs in the central field are transient. One of the remaining sources (r2-12) is highly variable (see figure 4). In Field 2, the disk field that is closest to the nucleus, 3 of 5 non-stellar SSSs are transient. In Field 1, located far out along the major axis, 1 of 5 non-stellar SSSs is transient and one is variable. None of the 5 non-stellar SSSs in Field 3 has been found to be transient or variable. The result could have been different had *XMM* observed a longer portion of Field 3. The small S values in this field may, however, suggest a lower level of variability than in the other fields.

7. LOCATION

The location of SSSs, and the stellar populations within which we find them, can provide important clues as to the natures of the sources. Old sources are likely to be scattered through the galaxy, wandering through its disk, bulge and halo. The standard models of SSSs would tend to predict that SSSs should be old, or at least intermediate-age systems. This is because the time at which mass starts being transferred to a WD at high rates ($\sim 10^7 M_\odot$ yr^{-1}), is generally governed by the evolution time of the donor. For both close binary SSSs and for symbiotics, donor masses are typically $\sim 1.5-2 M_\odot$ (Rappaport et al. 1994, Kenyon 1986); in the former case, the donor is slightly evolved and in the latter, it is very evolved. Novae, which can appear as SSSs, are also generally old systems.

Young sources can be found only in regions containing signatures of recent star formation: OB associations, HII regions, and SNRs. For example, in 10^6 years, a system traveling at 100 km s^{-1} can travel 100 pc, or about 27″ at the distance to M31. If, therefore we find density enhancements of SSSs close to young stars ($\leq 1'$), it is very likely that some of those SSSs are young. It is possible that some hot WD could be young systems– e.g., if they are PN descendants of $\sim 8 M_\odot$ stars, or if they accrete winds from a high-mass star.

Similarly, if some SSSs are formed close to the galaxy's center through the tidal disruption of giants, and if they remain supersoft for a few times $\sim 10^6$ years, then they must be found within a few hundred pc of the nucleus.

Below we establish that there are SSSs in the bulge, disk and halo of M31 and that their locations are such that some may be young systems while others may be old. This study by itself cannot, however, establish relative densities of sources in the bulge, disk and halo. This is because the effects of an intervening gas column are so powerful in hiding SSSs, lowering the count rate, or altering their spectra, that we need to couple the

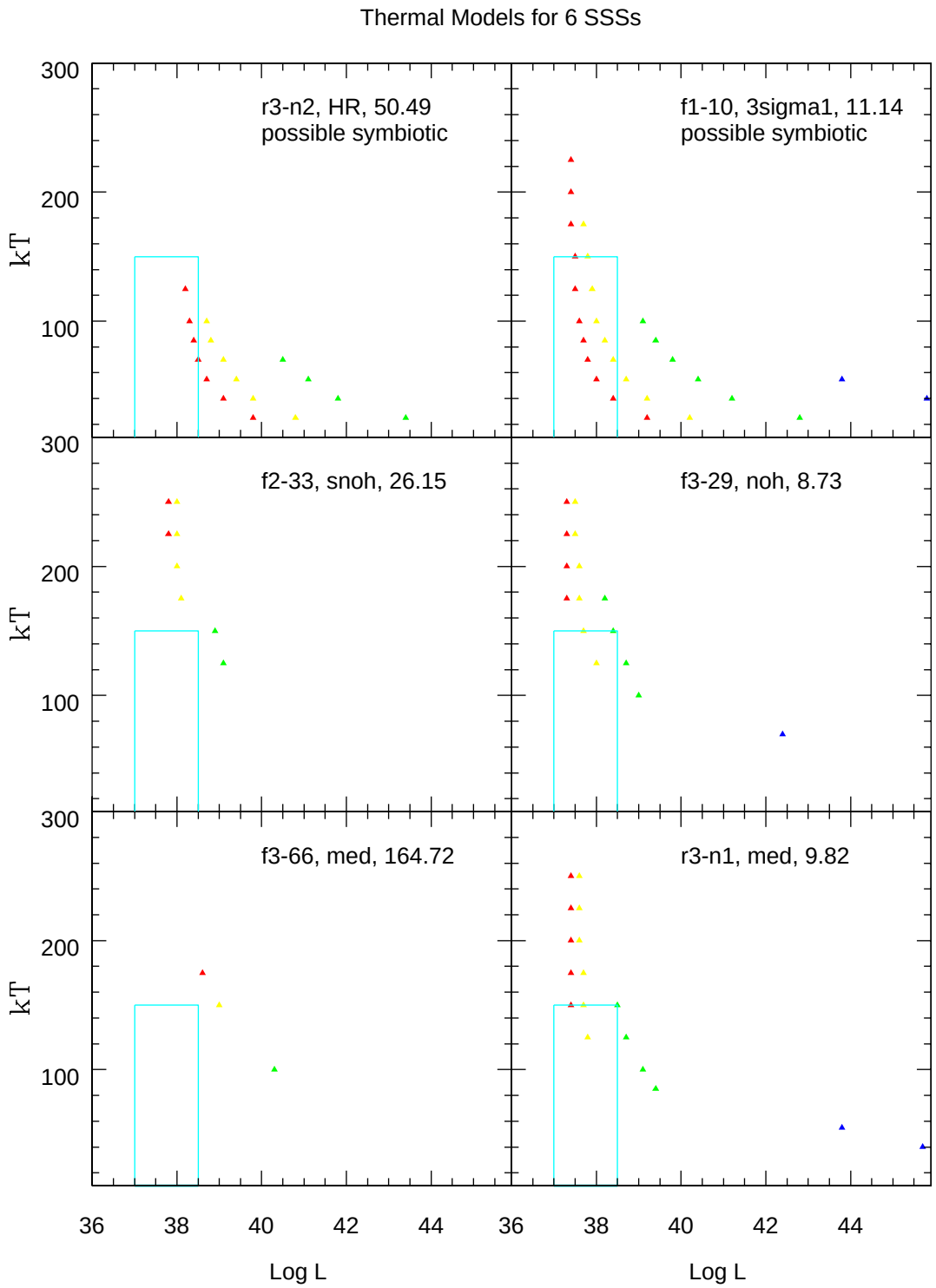

FIG. 5.— kT versus $Log(L_x)$ for 6 of the SSSs we identified in M31. Each triangle represents a model consistent with the total counts and broadband spectral distribution of the source. Models were computed for 4 values of N_H: 4.0×10^{20} cm^{-2} (red triangles), 1.6×10^{21} cm^{-2} (yellow triangles), 6.4×10^{21} cm^{-2} (green triangles), 2.5×10^{22} cm^{-2} (blue triangles). The cyan boxes represent the regions in the $L-T$ plane roughly consistent with nuclear burning models. In each panel, the label on the upper right shows the source name, the set of selection criteria that identified it as an SSS, and the total number of counts.

X-ray observations with detailed maps of the column density distribution.

7.1. *Bulge Sources*

Before we observed M31, it was not clear whether SSSs would be found in galaxy bulges. High Galactic absorption prevents us from detecting them in the bulge of the Milky Way. Predictions were difficult, not only because of uncertainties in the models, but also because the stellar populations near the center of galaxies like the Milky Way and M31 are complicated; old stellar populations are expected, but there is also evidence of recent and ongoing star formation.

ROSAT discovered only 1 SSS in the central kpc. *Chandra* finds 14 SSSs in the central $8' \times 8'$. Two of these are within a projected distance of 100 pc of the galaxy center, and an additional 8 SSSs lie within a projected distance of ~ 450 pc of the center.

The earliest *Chandra* observation of M31 discovered an SSS within $2''$ of nucleus. Given the value of the SSS spatial density, the probability of an SSS being within a few pc of the nucleus is very low. It therefore seems likely that the source is somehow related to the presence of the nucleus. A natural explanation is that the SSS is the hot core of a giant that was tidally stripped by the massive central ($3 \times 10^7 M_\odot$) BH. Some of the 10 sources within ~ 450 pc of the nucleus could potentially be stripped cores of giants, which have had time to move from the galaxy center. Statistical studies of a broad range of galaxies, as well as further work on M31, e.g., comparing the spatial density distribution of SSSs with other X-ray sources near the galaxy center, may help to verify or falsify this hypothesis. It is also possible that the centrally located SSSs are interacting binaries descended from the young and old populations that inhabit the bulge.

The SSSs in the bulge have higher average and median count rates than those in the disk. The average and median and highest count rates for the central field are 8.7 ks^{-1} and 2.6 ks^{-1} and 69.3 ks^{-1}, respectively. For Fields 1, 2 and 3, the corresponding triplets of numbers (average, median, and high count rates) are (0.79 ks^{-1}, 0.35 ks^{-1}, 1.38 ks^{-1}), (0.96 ks^{-1}, 0.83 ks^{-1}, 1.83 ks^{-1}), and (1.49 ks^{-1}, 0.57 ks^{-1}, 4.31 ks^{-1}), respectively. The bulge SSSs are also generally softer, as witnessed by the fact that a larger fraction of them are identified by the HR condition (8 HR sources out of 16 bulge sources. There are 1, 1, and 0 HR source out of 5, 5, and 6 non-stellar SSSs in Fields 1, 2, and 3, respectively).

7.2. *Disk Sources*

Because of M31's tilt relative to our line of sight, it is difficult to identify any particular source as a disk source, rather than a member of the halo. Nevertheless, the clustering of SSSs in Field 2 near regions with young stars, as delineated in Figure 1 by the presence of SNRs, indicates that some of these SSSs are likely members of the disk population. All 5 non-stellar SSSs in Field 2 are clustered near regions of star formation. One, f2-53, is in fact itself a SNR. Three of the others are transient and are probably X-ray binaries. If their location near SNRs is genuine, and is not due to projection effects, such SSSs are likely to be young systems.

7.3. *Halo Sources*

The SSS in Field 3 which is positioned farthest from the major axis of the disk is f3-66. At $\sim 32'$, or ~ 4.8 kpc from the major axis, and $\sim 56'$, or almost 14 kpc, from the nucleus, this source is likely to be in the halo of M31. Other non-stellar sources, including f3-46 and f3-31, are also far enough away from the disk to be members of halo. Some SSSs in Field 1 are as far as $\sim 80'$ (18 kpc) from the nucleus, and are also likely to be halo sources. These include f1-10, which is a good candidate for a symbiotic system. Its location in the halo is consistent with the fact that symbiotics can be members of old populations.

8. QUASI-SOFT SOURCES

In order not to miss some of the highest-T "classical" SSSs, those most likely to be high-mass accreting WDs, we had to assume the risk of selecting sources of even higher temperature than we had originally wanted. [9]

In Figure 5 we present examples of the ranges of temperatures and luminosities of sources selected by our algorithm. Because we had too few counts to fit spectra, we used a comparison of the data, binned into our 3 broad spectral bands, with models. Count rates for the models had been computed using the PIMMS software. We attempted to match the total counts and distribution of counts in S, M, and H, with models that had been computed by PIMMS. Each model is a black body characterized by a temperature, luminosity, and value of N_H (The PIMMS models should be roughly consistent with the detector sensitivity of AO2.) If the count rates in each band agreed with the model (within the 1σ uncertainty limits), we considered the model to be a possible match. Each match is represented by a triangle in the figure. Models were computed for 4 values of N_H : 4.0×10^{20} cm^{-2} (red triangles), 1.6×10^{21} cm^{-2} (yellow triangles), 6.4×10^{21} cm^{-2} (green triangles), 2.5×10^{22} cm^{-2} (blue triangles). The cyan boxes represent the regions in the $L-T$ plane roughly consistent with nuclear burning models. Although these model matches are not as reliable as spectral fits, they do suggest which SSSs may be classical supersoft sources (cSSs) and which may be quasi-soft sources (qSSs).

Interestingly enough, f1-10, the possible symbiotic, appears to be consistent with the WD models. The other possible symbiotic, r3-n2 may also be consistent with WD models, although the case is less clear. The other sources, selected by the "med", "noh", and "snoh" conditions, are almost certainly not consistent with WD models, and the fact that their broadband spectra seem compatible with values of kT$>$ 175 eV indicates that they are likely to be quasi-soft (see §3).

These quasi-soft sources could be neutron stars, or WDs with a harder spectrum than anticipated, perhaps due to upscattering of photons from the WD. A natural explanation is provided by an optically thick, geometrically thin disk around an accreting black hole. If we identify the source temperature with the temperature of the inner disk, located at the radius of the last stable orbit, and assume that 10% of the accretion energy is emitted, then the mass of the BH accretor is given by

$$M_{BH} = 10^3 M_\odot \left[\frac{49\,eV}{kT}\right]^2 \left[\frac{L}{2.9 \times 10^{37} erg/s}\right]^{\frac{1}{2}} \qquad (4)$$

For kT = 200 eV, and $L = 1 \times 10^{38}$ erg s^{-1}, the BH mass is roughly $100\,M_\odot$. This value of the mass is likely to be a lower limit, since spectral hardening effects, orientation effects, and spin would all tend to increase the derived value of

[9] It is interesting to note that we find that some of the SSSs selected by the strictest criteria, the HR conditions, are best fit by models that include a power-law component in addition to a soft thermal spectrum. See Figure 2.

the mass. This example illustrates that some of the quasi-soft models could be accreting intermediate-mass BHs. It is important to note that even the softest sources could be accreting intermediate-mass BHs. (See Equation 4.) Figure 5 simply illustrates that there are some soft sources in M31 that may be inconsistent with WD models; these are then the most obvious candidates for other models, such as the BH model.

9. LUMINOSITY DISTRIBUTIONS

In each field, there are SSSs with count rates below 1 ks^{-1}. In Field 1, the 2 lowest count-rate sources have count rates of 0.27 ks^{-1} and 0.35 ks^{-1} . In each of Fields 2 and 3 there are 3 sources with count rates ranging from 0.22 or 0.34 ks^{-1} to ~ 1 ks^{-1}. In Field 2, there are 5 sources with count rates below 1 ks^{-1}.

Because the luminosity, temperature, and column density each play a crucial role in determining the count rates of SSSs, the low-count-rate sources undoubtedly represent a range of source luminosities. For the AO2 observations, the range of SSS luminosities of the low-count-rate sources was between $\sim 10^{35}$ erg s^{-1} (for a 100 eV source behind a column of 7×10^{20} cm^{-2}), to just over 10^{36} erg s^{-1} (for a 50 eV source behind a column of 1.5×10^{21} cm^{-2}).

Although we cannot determine which among our sources have the lowest luminosities, we can definitively say that we are detecting sources with luminosities below 10^{37} erg s^{-1}. The significance of this number is that it represents the luminosity of an $0.6 M_{\odot}$ WD that is burning hydrogen to helium in a quasi-steady manner. We conjecture that at least some of the lower luminosity sources may correspond to WDs of lower mass and on/or bright CVs (Greiner et al. 1999, Greiner & Di Stefano 1999, Patterson et al. 1998).

10. CONCLUSIONS

Our work with M31 demonstrates the challenges and rewards of studying SSSs in other galaxies. The primary challenge is posed by the low count rates, making it difficult to select sources based on spectral criteria. For SSSs the situation is complicated because (1) we don't know *a priori* whether one or more physical models apply, and (2) for any specific physical model, we cannot uniquely predict the spectrum from the accretor, disk, corona, interactions with the ISM, etc. We have therefore chosen to develop and apply an algorithm for source selection that has been tested on simulated and real data from other galaxies. [10] (See Di Stefano & Kong 2003a, 2003b.) The algorithm categorizes sources according to the details of how they were selected, allowing us to select those most likely to be intrinsically soft. Future investigations can now focus on any subset of the SSSs identified by our algorithm.

In M31 we find 33 SSSs that are not foreground stars. Five of these are in Field 1, five are in Field 2, seven are in Field 3,and sixteen are in the central field. Comparative studies of the *ChaMP* fields to estimate the numbers of background SSSs indicate that all of these sources are likely to be in M31.Two of the sources (r2-56 and f2-53) appear to be associated with SNRs. One of these, r2-56, is resolved at X-ray, optical, and radio wavelengths. This SNR exhibits no emission above 1.1 keV and was selected by the HR conditions, the strongest selection criteria. F2-53 satisfies the 3σ criteria, the second strongest set of selection criteria.

The sixteen bulge SSSs include the brightest, softest SSSs in M31. The bulge sources are highly concentrated within a projected distance of 450 pc from the galaxy center. The surface density and count rates of SSSs in the disk field are smaller, and the sources are, on average, harder than those in the bulge. It remains to be seen if the differences between the disk and bulge are due to greater absorption in the disk or if they are intrinsic to the sources.

M31's SSSs are highly variable. Thirteen out of 15 (non-SNR) bulge SSSs rose above or fell below the *Chandra* and *XMM* detectability limits on time scales of months, as did 3 of 5 non-stellar SSSs in Field 2. There have been fewer checks for variability in Fields 1 and 3, as they were not covered by *XMM*. Nevertheless, 8 of the 8 *ROSAT* SSSs scattered across Fields 1, 2 and 3 that could be checked for variability had faded below detectability between 1991 and 2000/2001. The fading of the SSSs that have fallen below the detectability limits cannot be explained by assuming that the SSSs are novae. The required rate of novae would be too high to be compatible with other data (Shafter & Irby 2001). Furthermore we find sources turning on as well as turning off, with on-off-on or off-on-off behavior observed for some SSSs. The most viable conjecture is that the variable SSSs are X-ray binaries.

Disk SSSs in Field 2 appear to be clustered near star-forming regions, indicating that they may be young systems. Others appear to be in the halo of M31 and may be old. The results match what we have seen in other galaxies. In M101, e.g., which we view face-on, SSSs are predominantly found in the spiral arms, (Di Stefano & Kong 2003a, b). In M104 (the Sombrero), on the other hand, which we view edge-on, some SSSs are clearly located several kpc away from the disk.

In the center and disk we find SSSs with count rates between 0.25 and 1 counts ks^{-1}. These are likely to have luminosities between $10^{35} - 10^{37}$ergs^{-1}, lower than those of the Magellanic Cloud and Galactic SSSs that defined the class through *ROSAT* observations in the early 1990's. Some of these sources may be bright CVs with relatively high accretion rates (Greiner and Di Stefano 1999, Greiner et al. 1999, Patterson et al. 1998).

Considering all of the fields we studied, 10 SSSs were discovered by the HR condition and 5 by the next most selective criteria, the 3σ conditions. Eighteen non-stellar sources satisfy conditions that are somewhat less strict. Twelve of these exhibit no significant emission above 2 keV (6 "noh" sources and 6 "med"), and 6 allow some emission in the H band, as long as the fraction of such photons is small. Some could be accreting intermediate-mass black holes; some may be quasi-soft.

The regions containing the largest numbers of detectable SSSs are the four $8' \times 8'$ squares covered by S3. Even in each of Fields 1 and 3, far from the nucleus, there are 3 non-stellar SSSs in S3. In regions close to but not overlapping the nucleus, the numbers of sources in an $8' \times 8'$ field should lie between 3 and 16. If we consider that there are $>$ forty $8' \times 8'$ fields within D25, and assume that each houses four SSSs, an A02 S3 survey of M31 would have detected > 300 SSSs. To derive the total underlying population, absorption effects need to be taken into account; this will be done separately.

In terms of the properties and possible natures and origins, the SSSs of M31 are a more diverse group than we had anticipated. *HST* ACS observations to identify dim optical counterparts, *XMM* data on the disk fields, and *Chandra* observations

[10] The other galaxies were chosen because there is little absorption along the line of sight to them and in some cases (e.g., M101, M83), the orientation is more face-on than M31's, hence is favorable for the detection of SSSs.

of the region will help us to unravel the mystery of their fundamental natures.

This work was supported by NASA under an LTSA grant, NAG5-10705. A.K.H.K. acknowledges support from the Croucher Foundation. R.D. would like to thank P. Green & P. Plucinsky for discussions and R. Remillard for providing access to an unpublished paper.

REFERENCES

Blair, W.P., & Long, K.S. 1997, ApJS, 108, 261
Ciardullo, R. & Jacoby, G.H. 1998, Bulletin of the American Astronomical Society, 30, 1275
Deharveng, L., Caplan, J., Lequeux, J., et al. 1988, A&AS, 73, 407
Dickey, J.M., & Lockman, F.J. 1990, ARA&A, 28, 215
Di Stefano, R., & Rappaport S. 1994, ApJ, 437, 733
Di Stefano, R. & Nelson, L. A. 1996, LNP Vol. 472: Supersoft X-Ray Sources, 3
Di Stefano, R., Kong, A.K.H., Garcia, M.R., Barmby, P., Greiner, J., Murray, S.S., & Primini, F.A. 2002a, ApJ, 570, 618
Di Stefano, R., Greiner, J., Kong, A., Garcia, M.R., Primini, F.A., Barmby, P., Murray, S.S., Curry, S. 2002b, American Physical Society, APRN17072
Di Stefano, R., & Kong, A.K.H. 2003, ApJ, in press (astro-ph/0301162), DK03
Di Stefano, R., & Kong, A.K.H. 2003c, in preparation
Frank, J., King, A., & Raine, D.J. 2002, Accretion Power in Astrophysics: Third Edition, CUP
Freedman, W.L., et al. 2001, ApJ, 553, 47
Freeman, P.E., Kashyap, V., Rosner, R. & Lamb, D.Q. 2002, ApJ, 138, 185
Friedman, R.B., Di Stefano Kong, A.K.H., Barmby, P., Kundu, A. 2002, American Astronomical Society Meeting, 201
Greiner J., Hasinger, G. & Kahabka, P. 1991, A&A, 246, 17
Greiner J., Tovmassian G.H., Di Stefano R., Prestwich A., Gonzalez-Riestra R., Szentasko L., Chavarria C., 1999, Transient supersoft x-ray emission from V751 Cygni during optical low-state, A&A, 343, 183
Greiner, J. & Di Stefano, R. 1999, Highlights in x-ray astronomy : international symposium in honour of Joachim Trümper's 65th birthday, June 17-19, 1998, Garching, Germany : symposium proceedings / edited by Bernd Aschenbach & Michael J. "Freyberg."Garching : Max-Planck-Institut für extraterrestriche Physik, 1999. MPE report, No. 272, ISSN 0178-0719), p.66, 66
Greiner, J. 2000, NewA, 5, 137
Greiner, J., & Di Stefano, R. 2002, ApJ, 578, L59
Hachisu, I., Kato, M., Nomoto, K. 1996, ApJ, 470, L97
Kaaret, P. 2002, ApJ, 578, 114
Kahabka, P., Pietsch, W., & Hasinger, G. 1994, Supersoft X-Ray Sources in the Fields of the Magellanic Clouds, A&A, 288, 698
Kahabka, P. 1996, A&A, 306, 795
Kahabka, P. 1999, A&A, 344, 459
Kenyon, S. J. 1986, Cambridge and New York, Cambridge University Press, 1986, 295
Kylafis, N.D. & Xilouris, E.M. 1993, A&A, 278, 43
Kong, A.K.H., Charles, P.A., & Kuulkers, E. 1998, NewA, 3, 301
Kong, A.K.H., Garcia, M.R., Primini, F.A., Murray, S.S., Di Stefano, R., & McClintock, J. 2002, ApJ, 577, 738
Kong, A. K. H., Di Stefano, R., Garcia, M. R., & Greiner, J. 2003, ApJ, 585, 298
Kong, A. K. H.& Di Stefano, R. 2003, ApJ, 590, L13
Kong, A.K.H., Sjouwerman, L.O., Williams, B.F., Garcia, M.R., Dickel, J.R. 2003, ApJ, 590, L21
Lomb, N.R. 1976, Ap&SS, 39, 447
Long, K.S., Helfand, D.J., & Grabelsky, D.A. 1981, A Soft X-Ray Study of the Large Magellanic Cloud, ApJ, 248, 925
Magnier, E.A., Primini, F.A., Prins, S., van Paradijs, J. & Lewin, W.H.G. 1997, ApJ, 490, 649
Morgan, D.H. 1996, MNRAS, 279, 301
Mukai, K., Pence, W.D., Snowden, S.L., Kuntz, K.D. 2003, ApJ, 582, 184
Nedialkov, P., Orio, M., Birkle, K., Conselice, C., Della Valle, M., Greiner, J., Magnier, E., & Tikhonov, N. A. 2002, A&A, 389, 439
Parmar, A., Kahabka, P., Hartmann, H.W., Heise, J., Martin, D.D.E., Bavdaz, M., & Mineo, T. 1997, A BeppoSAX Observation of the Super-Soft source CAL87., A&A, 323, L33
Patterson J., Kemp J., Shambrook A., Thorstensen J.R., Skillman D.R., Gunn J., Jensen. L., Vanmunster T., Shugarov S., Mattei J.A., Shahbaz T., Novak R., 1998, PASP 110, 380
Pence, W.D., Snowden, S.L., Mukai, K., & Kuntz, K.D. 2001, ApJ, 561, 189
Pietrzynski, G., Gieren, W., Fouque, P., & Pont, F 2001, A&A, 371, 497
Popham, R., & Di Stefano, R. 1996, in Supersoft X-Ray Sources, Proceedings of the International Workshop Held in Garching, Germany, 28 February - March 1996. Lecture Notes in Physics, Vol. 472, edited by Jochen Greiner. Springer-Verlag, Berlin Heidelberg New York, p.65
Primini, F., Forman, W. & Jones, C. 1993, ApJ, 410, 615
Primini, F., Magnier, E. & Hasinger, G. 1997, Bulletin of the American Astronomical Society, 29, 1292
Rappaport, S., Di Stefano, R. & Smith, J.D. 1994, ApJ, 426, 692
Read, A.M., Ponman, T.J., & Strickland, D.K. 1997, MNRAS, 286, 626
Read, A.M., & Pietsch, W. 2001, A&A, 373, 473
Sarazin, C.L., Irwin, J.A., & Bregman, J.N. 2001, ApJ, 556, 533
Shafter, A.W. & Irby, B.K. 2001, ApJ, 563, 749
Southwell, K.A., Livio, M., Charles, P.A., O'Donoghue, D., & Sutherland, W.J. 1996, The Nature of the Supersoft X-Ray Source RXJ0513-69, ApJ, 470, 1065
Supper, R., Hansinger, G., Pietsch, W., Truemper, J., Jain, A., Magnier, E.A., Lewin, W.H.G. & van Paradijs, J. 1997, A&A, 317, 328
Supper, R., Hasinger, G., Lewin, W.H.G., Magnier, E.A., van Paradijs, J., Pietsch, W., Read, A.M., Trümper, J. 2001, A&A, 373, 63
Swartz, D.A., Ghosh, K.K., Suleimanov, V., Tennant, A.F., Wu, K. 2002, ApJ, 574, 382
Trudolyubov, S. P., Borozdin, K. N., Priedhorsky, W. C., Mason, K. O., & Cordova, F. A. 2002, ApJ, 571, L17
Tully, R. 1988, Nearby Galaxies Catalog (Cambridge: Cambridge Univ. Press)
van Teeseling, A., Heise, J., & Kahabka, P. 1996 *Compact Stars in Binaries*, eds. J. van Paradijs et al., 445
van Teeseling, A., & King, A.R. 1998, A&A, 338, 957
van den Heuvel, E.P.J., Bhattacharya, D., Nomoto, K., & Rappaport, S.A. 1992, Accreting White Dwarf Models for CAL 83, CAL 87 and Other Ultrasoft X-Ray Sources in the LMC, A&A, 262, 97
White, N. E., Giommi, P., Heise, J., Angelini, L., & Fantasia, S. 1995, ApJ, 445, L125
Williams, B. F. et al. 2003